11^{th} International Conference on Fracture Mechanics of Concrete and Concrete Structures
FraMCoS-11
J. M. Chandra Kishen, A. Ramaswamy, S. Ray and R. Vidyasagar (Eds)
https://doi.org/10.21012/FC11.0923107

TIME FUNCTION ANALYSIS OF ACOUSTIC EMISSIONS GENERATED DURING COMPRESSIVE FRACTURE PROCESS IN STEEL FIBER REINFORCED CONCRETE

NIKHIL GUPTA[1*], R. VIDYA SAGAR[1†] AND J. M. CHANDRA KISHEN[1‡]

[1]Department of Civil Engineering,
Indian Institute of Science, Bangalore-560012,India.
*e-mail: nikhilgupta1@iisc.ac.in
†e-mail: rvsagar@iisc.ac.in
‡e-mail: chandrak@iisc.ac.in

Keywords: Steel Fiber Reinforced Concrete, Acoustic Emission, Time to failure, Inter-event time, Sliding time window, Accelerated deformation law

Abstract. This article presents a study on the 'time evolution of acoustic emissions (AE)' in terms of time-to-failure to understand the compressive fracture process in Steel Fiber Reinforced Concrete (SFRC). In other words, the study focuses on how generation of AE changes with time. Several unconfined uniaxial compression tests were conducted in the laboratory on specimens with varying fiber content (V_f), and simultaneously, the generated AE were recorded. The present study considered time function (F) which is based on inter-hit time intervals to distinguish between different fracture stages involved in the compressive fracture process. The pre-peak behavior and post-peak behavior is analyzed separately on the logarithmic scale, providing a magnified view of fracture process at all the loading stages. The evolution of F over time reflects a recurring set of qualitative features for each V_f. The F involves the optimized selection of a sliding time window as it describes the resolution of the analysis. Thus, the variation of the sliding time window for F was also studied. The F was observed to be governed by a power law, with the exponent varying in proportion to V_f. The scaling described by power law is in accordance with the accelerated deformation law observed in seismology, which substantiates the universality law. The interpretation of the AE data provides useful information on pre-failure indication and contributes to an understanding of the mechanical behavior of SFRC.

1 INTRODUCTION

Steel Fiber Reinforced Concrete (SFRC) is a composite material composed of cementitious matrix and discrete steel fibers. The material exhibits improved mechanical properties compared to the conventional concrete, such as enhanced ductility, crack resistance, tensile and flexural strength [1] . The inclusion of steel fibers provides a secondary reinforcement mechanism that contributes to the overall performance of SFRC [2]. However, understanding the fracture process of SFRC under three modes of fracture and different loading conditions is important for designing structures that utilize the material effectively. The acoustic emission (AE) testing has been acknowledged for quite some time as an immensely useful non destructive testing method for monitoring and quantification of dynamic processes within various contexts [3, 4]. The information yielded through applying the AE testing enables the understanding of fracture mechanisms. Moreover, the technique offers prompt cautionary indications of impending failure [5].

Studying AE in a controlled laboratory settings enables to understand the evolution of fracture. This also allows to formulate valid and applicable laws for large-scale structures [6]. The distribution of various AE waveform hit parameters and investigation is anticipated to adhere to universal principles. This universality facilitates the transfer of physical observations from one scenario to another [7]. An essential attribute of quasi-brittle materials is their inherent heterogeneity, resulting in damage manifesting as microcracks. These microcracks give rise to the creation of intricate pathways and induce structural instability within stressed concrete.

1.1 Literature Review

AE testing has gained significant attention in studying the behavior of SFRC under various loading conditions [3]. Researchers have utilized AE to monitor crack initiation and propagation, fiber-matrix interactions, and other internal changes within SFRC specimens [8]. The ability of AE to provide real-time data on the development of microcracks and structural changes has proven valuable in understanding the mechanical response of SFRC [9].
The analysis of AE data from SFRC involves several techniques. The AE Source location analysis, which identifies the spatial position of acoustic emission events, aids in understanding crack propagation paths. Peak Amplitude - frequency of occurrence provide insights into the severity of damage [10]. The pattern recognition and statistical analysis is useful to classify and categorize different acoustic signals, leading to a better understanding of the material's behavior [11]. The statistical information extracted from AE data has provided valuable insights to investigate the sequences leading to failure and the fracture process in both concrete and rock materials [12]. A comprehensive advancement of data related to the average frequency (AF) and the rise time (RT) of acoustic signals enables accurate categorization of tensile cracking and shear cracking. This categorization is based on whether the fracture is caused by microcracking under tension (Mode-I), shear (Mode-II), or a combination of both, known as mixed-mode phenomena [9].
The application of AE testing to study the fracture process in SFRC remains a prominent area of interest for researchers as they seek comprehensive insights from different perspectives. Additionally, an alternative methodology for representing the AE data is the utilization of a time function. This technique has been employed in previous studies, particularly in the context of brittle materials like rocks and marble [13].

1.2 Research Significance

This article delves into the internal fracture mechanism when SFRC undergoes unconfined uniaxial compression. It employs experimental testing and analysis to understand the crack initiation, propagation, and post-cracking behavior of SFRC under compressive loading. This research provides insights into the fracture mechanics of SFRC, which are crucial for designing and optimizing structural elements in various engineering applications.

1.3 Aim of the study

This study aims to characterize the fracture mechanism stages occurring in SFRC using a relatively new approach to represent AE data. Generally, AE data analysis in existing literature follows a conventional approach. However, this study introduces a time function (F) to analyze the data. The variations of this function are studied at every stage of failure to investigate the fracture mechanisms involved.

2 METHODOLOGY

Applying mechanical loads induces increase in potential energy of the structures upto a certain extent. Further increase in load on the structure leads to development of yielding and fracture. This fracture leads to localized alteration in the material. The modification arises from fracture mechanisms within the structure, including the initiation, propagation, and coalescence of microcracks. It is established that distinct fracture mechanisms are accountable

for generating acoustic signals with varying features. Consequently, a diverse range of parameters associated with the corresponding acoustic waves are identified to simplify the analysis of acoustic activity. This enables the investigation of the individual fracture mechanisms using AE waveform data.

In this context, the depiction and detailed explanation of AE activity is accomplished by introducing a time function $F(\tau)$. This function encapsulates the mean frequency of AE hits occurring within a time window containing N successive hits. The function relies on the inter-event times between the consecutive hits. The hit time intervals of all the hits observed in the experimental investigation for each specimen are computed as follows:

$$\Delta t_j = t_j - t_{j-1} \qquad j = 2, 3, 4, ... \tag{1}$$

Here, t_j and t_{j-1} denote the moment when two successive hits occur. Subsequently, the average of inter-hits time, represented as τ, is computed for the N inter-hits times (Δt_j) within each set of N successive hits. These sets are referred to as τ_j and are calculated as:

$$\tau_j = \frac{t_{N+j-1} - t_{j-1}}{N}, \quad j = 2, 3, 4, ..., (H - N)$$
$$\tau_1 = \frac{t_N - t_1}{N}, \qquad when \quad j = 1 \tag{2}$$

Here, H is the total number of hits observed in the experiment. The computation of τ_j requires subsequent N time hits. Thus, the iteration over j varies up to $H-N$ hits, excluding final N hits. Choice of N (sliding time window) relies on the test being conducted and the data collected during the experiment. The present study determines the N by generating a probability density function (PDF) of the average time τ_j for various N. After a specific N, a consistent pattern is observed in the PDF and as a result, N is chosen larger than that value. The mean frequency of AE hits occurring within a designated time window spanning from t_j to t_{j+N} is denoted as time function $F(\tau)$. $F(\tau)$ is defined as the inverse of τ_j, which is the average inter-hits time for j^{th} window. Thus,

$$F(\tau_j) = \tau_j^{-1} \qquad j = 1, 2, \ldots, (H - N) \tag{3}$$

Every $F(\tau_j)$ is associated with $\bar{t}_j$ which is the mean of the time moments of the corresponding N hits. It is observed that the PDF of τ_j doesn't exhibit a Gaussian distribution. Hence, the mean value is determined by the median of each sliding window.

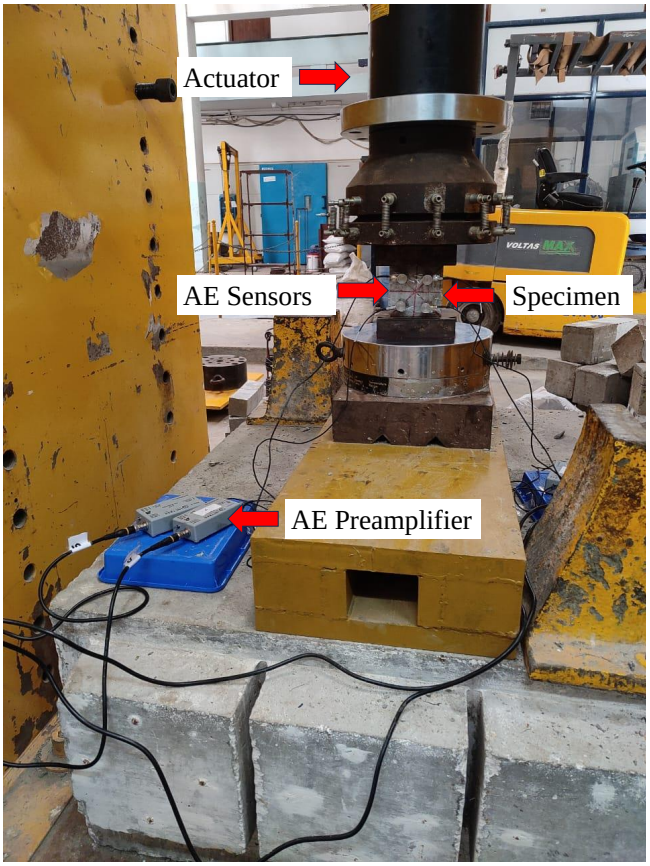

Figure 1: Experimental Setup in structures laboratory, Department of Civil Engineering, Indian Institute of Science, Bangalore

3 EXPERIMENTAL PROGRAM

Steel fiber reinforced concrete specimens with similar geometry and mix design but different fiber content were prepared. The samples were prepared following the ACI 544 code. Two end-hooked steel fibers (diameter is 0.55 mm, length is 30 mm, and tensile strength is 1269 MPa), ordinary Portland cement, 10 mm coarse aggregate and river sand as fine aggregates were utilized to cast the specimen. The

test specimens are in cubical shape having each side of 100 mm with three distinct volume fractions of fiber V_f (0.8%, 1.2% and 1.6%) which are tested under unconfined uniaxial compression at a loading rate of 0.004 mm/s. The testing uses displacement control loading to capture the post-peak response. The experimental setup comprised a servo-controlled hydraulic loading frame with a load capacity of 2000 kN as shown in Figure 1. The test is conducted until the load-carrying capacity of the specimen reduces to 70-80% of the peak load, denoted as time to failure in Table 1.

Table 1: Experimental data observed

$V_f(\%)$	S	P_m(kN)	TF(s)	H	E(V-s)
0.8	1	483.8	830	340734	1.7×10^7
	2	490.2	834	329437	1.9×10^7
	3	474.6	821	304532	1.4×10^7
1.2	4	549.4	1080	410087	2.5×10^7
	5	538.7	1064	432964	2.1×10^7
	6	552.3	1053	443829	2.6×10^7
1.6	7	555.3	1140	525066	1.1×10^7
	8	571.2	1134	513495	0.9×10^7
	9	562.2	1174	547823	1.2×10^7

V_f :Volume fraction of fiber; S: Sample Number; P_m:Peak Load; TF: Time to failure; H: Total hits observed; E: Total AE energy released

The generated AE waves are recorded using an eight-channel AE monitoring system. Four piezoelectric sensors (54 kHz resonant frequency) were mounted to the test specimen. The preamplifiers gain was set to 40 dB. The timing parameters, namely PDT (peak definition time), HDT (hit definition time), and HLT (hit lockout time), were configured to 200 µs, 800 µs, and 1000 µs, correspondingly. The AE detection threshold was set at 40 dB, and sensors are attached to conduct two-dimensional (2D) planar source localization.

4 RESULTS AND DISCUSSION

The recorded peak load, time to failure, number of total hits, and total AE energy released for each specimen are given in Table 1.

4.1 Influence of steel fiber content on mechanical behavior of SFRC and generated AE

The mean value of the peak load (P_m) of the specimens indicates that the addition of fibers has little impact on the compressive strength of the specimens. Specifically, when the fiber content is raised from 0.8% to 1.2%, there is an increase in load-carrying capacity by approximately 13%. However, this increase is more modest when the fiber content is further elevated from 1.2% to 1.6%, resulting in a mere 3% increment in load-carrying capacity as shown in Table 1. The influence of fibers becomes apparent in the post-peak behavior of the specimen, where the initiation of fiber bridging tends to delay the formation of macrocracks for specimens with higher fiber content.
Subsequently, there is a noticeable increase in hits as the fiber content increases. The fibers act as bridging across the cracks, impeding their propagation and delaying their expansion. As a consequence, a greater quantity of microcracks are generated for higher fiber content, leading to an increased occurrence of hits. However, the highest mean total AE energy released is associated with the 1.2% fiber content. This energy decreases for 1.6% fiber content and is observed to be the lowest among the three fiber contents. This is because microcracks emit relatively low energy. In the case of the 1.6% fiber content, the macrocrack delay is marginally more pronounced, leading to an accumulation of greater microcracks and, consequently, a diminished overall release of AE energy. The observations have been validated and align with the existing literature [8], [14].

4.2 Fracture mechanisms in SFRC under uniaxial compression

In Figure 2, the variations in axial load over time for 0.8%, 1.2%, and 1.6% fibers, respectively, are depicted for the unconfined uniaxial compression test.

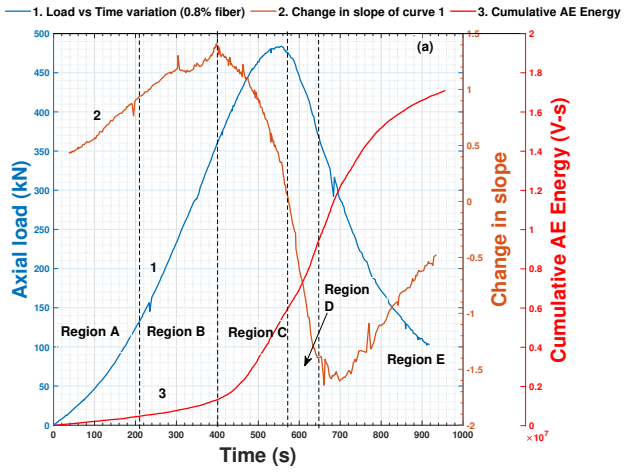

(a) $V_f = 0.8\%$

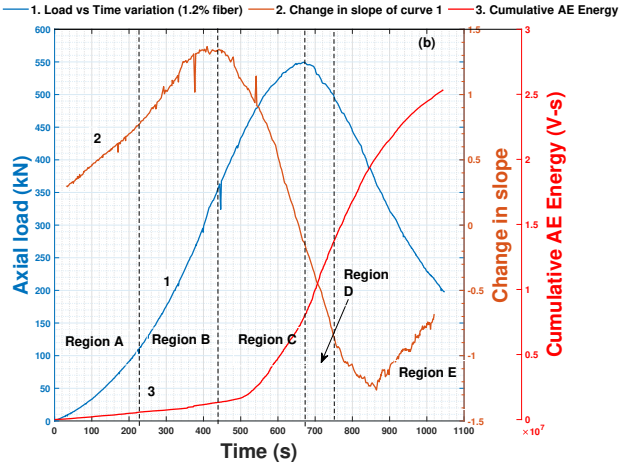

(b) $V_f = 1.2\%$

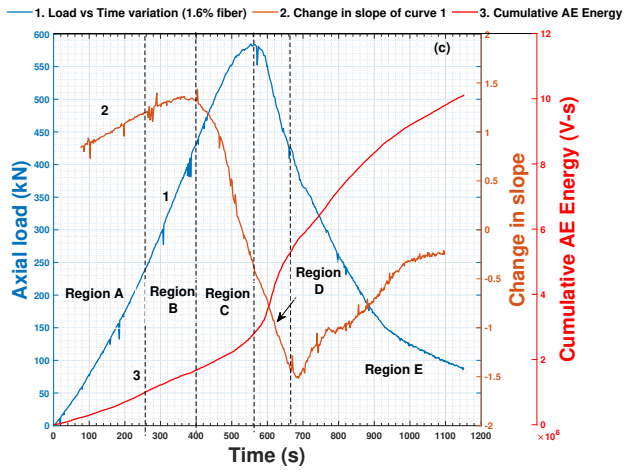

(c) $V_f = 1.6\%$

Figure 2: Variation of load and cumulative AE energy with time

The slope of the load variation curve with time and cumulative AE energy released are also included. The region namely A,B,C,D,E are selected based on the change in the load variation with time curve to understand the different fracture mechanisms. Region-A is designated as the initial compaction stage, during which the pores within the specimen are compressed, leading to a gradual yet discernible non-linear increase in load over time. The number of detected hits in this region is notably low, and these hits possess relatively low AE energy levels. Based on this, it can be inferred that microcracking has yet to occur in the specimen. The end of this region is marked by the point at which the load-time curve transitions to the elastic zone.

The subsequent region-B, represents the elastic compression stage. This stage is characterized by a progressive rise in the AE energy. This is because of microcracks forming within the cement matrix and the Interfacial Transition Zone (ITZ). The microcracks propagate stably, and no sudden fluctuations are observed in AE energy in this region.

In the following region-C, the load reaches its maximum, accompanied by a significant release of AE energy. The load variation becomes non-linear, indicating the coalescence of microcracks formed in the preceding region-B. As the load continues to increase consistently, these microcracks become macrocracks when the load reaches P_m. After the peak load is reached, the specimen experiences a loss in strength, reducing its load-carrying capacity.

The region following the peak load, characterized by a decline in load carrying capacity, is designated as Region-D. In this region, literature [8] suggests the evidence of fiber sliding. The fibers tend to align themselves with the macrocracks, impeding the propagation of cracks. The AE energy continues to rise as the macrocracks extend until the end of the region-D. The termination of this stage coincides with the initiation of the softening phase, denoted as Region-E.

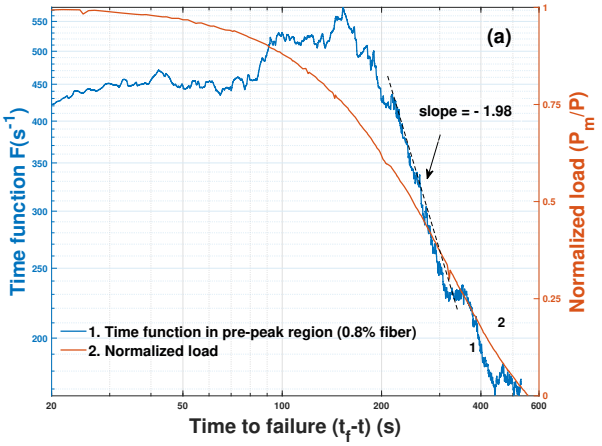

(a) $V_f = 0.8\%$

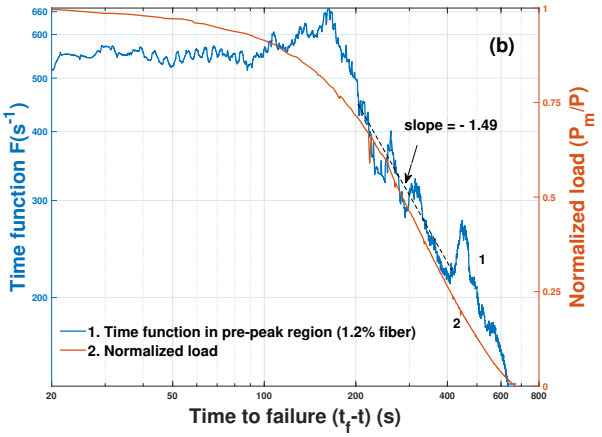

(b) $V_f = 1.2\%$

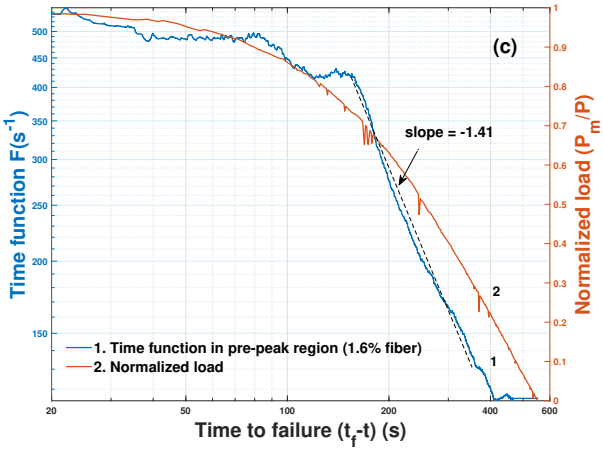

(c) $V_f = 1.6\%$

Figure 3: Variation of F and normalized load with time for pre-peak region in logarithmic scale

Within this region-E, the fibers role as bridging elements, preventing catastrophic failure of the specimen. The escalation in released AE energy is subdued due to the fibers bridging effect. Finally, the specimen's ultimate failure is observed, stemming from phenomena such as fiber pullout and aggregate breakage [8].

4.3 Time Function Analysis of AE

Inter-hit time intervals are computed for each sliding window (N). A kernel density plot of hit occurrence times is created for various N values to derive its PDF. Notably, when N is small, PDF for each sliding window exhibits considerable variability. However, after conducting a series of trials, it becomes evident that the variability diminishes when N surpasses 7000. Consequently, for this study, N is considered as 10000. The time function is computed using the equation 3 and N. The section 4.2 presented the fracture mechanisms and mechanical behavior of the SFRC specimen using a conventional approach. The time function is an alternate approach to represent it. The time evolution of $F(\tau)$ is plotted in the inverse time arrow (time to failure) using logarithmic scales along with the normalized load as shown in Figure 3 and 4. It is evident from the discussion in the section 4.2 that the mechanisms occurring in the pre-peak and post-peak region are different. Hence further analysis is performed separately for each V_f. It is observed that initial stages of fracture i.e. time to failure greater than 500s (load interval below $0.25P_m$) several fluctuations occur in $F(\tau)$. These fluctuations are stabilized for a short duration when the specimen is fully compacted. In the load interval between $0.25P_m$ to $0.75P_m$ the progressive increase in $F(\tau)$ is attributed to an intense growth of microcracks. Within this time interval the power law

$$F = B\left(t_f - t\right)^{-m} \tag{4}$$

perfectly describes the time variation of $F(\tau)$. Here, B is a constant and m denotes the exponent.

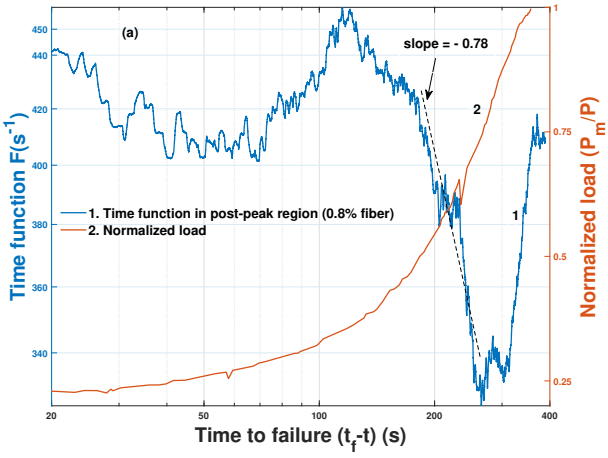

(a) $V_f = 0.8\%$

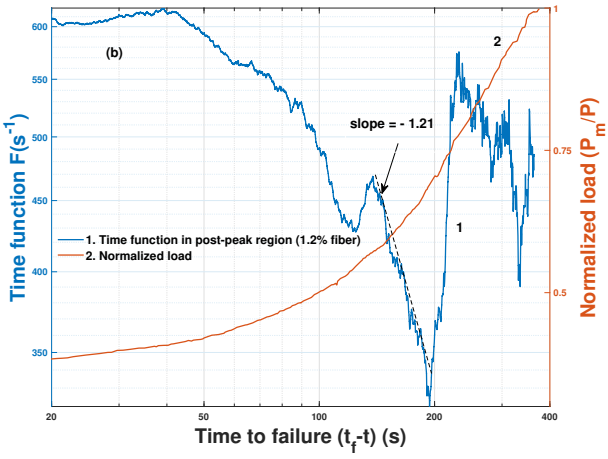

(b) $V_f = 1.2\%$

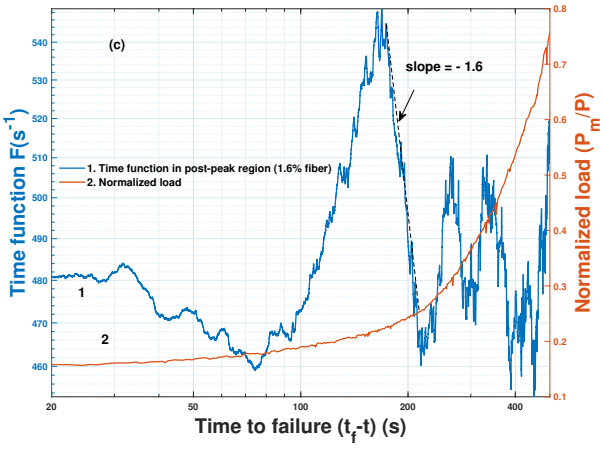

(c) $V_f = 1.6\%$

Figure 4: Variation of F and normalized load with time for post-peak region in logarithmic scale

The slope of this region in the logarithmic scale represents the exponent of power law. The slope is observed as -1.98, -1.49, -1.41 for V_f of 0.8%, 1.2% and 1.6% respectively. The slope quantifies the higher frequency of microcracks generating in 0.8% V_f. Function F attains a maximum value and saturates after this time interval (load interval after 75% of peak load). It signifies the coalescence of the microcracks and generation of the macrocracks. An analogous analysis is conducted in the work outlined in literature [13] pertaining to the pre-peak region within brittle materials. The outcomes demonstrate concurrence with the findings presented in literature [13]. Similar trends are observed in post peak analysis also. In post peak region the time interval of fiber crack bridging follows the power law with slope as -0.78, -1.21, -1.6 for fiber content 0.8%, 1.2%, 1.6%, respectively. The presence of high fiber content prevents the opening of macrocracks. During this process instead of macrocracks the initiation of new microcracks occurs. Thus, a higher amount of hits is observed for higher fiber content. This is justified by the slope values obtained in the analysis.

The observed behavior in the SFRC specimen aligns with the principles of the accelerated deformation law within seismology [15]. This law pertains to the accelerated movement along a fault line attributed to the progressive accumulation of stress over time. It can be asserted that the agreement of this phenomenon with the AE data demonstrates the correlation existing among distinct-scale physical processes. As a result, the scaling of the time function proves to be universal across both AE data and earthquake phenomena.

4.4 Effect of sliding time window

The time function presents the frequency of hits observed during the mechanical loading of the specimen. It includes the user input sliding window which describes the resolution of the analysis. The variation of parameter N is examined and depicted in Figure 5. The $F(\tau)$ trend remains consistent across the range of N

from 1000 to 10000; however, higher N values yield smoother results. Thus, enhancing the resolution of the plot through a higher N value improves comprehension.

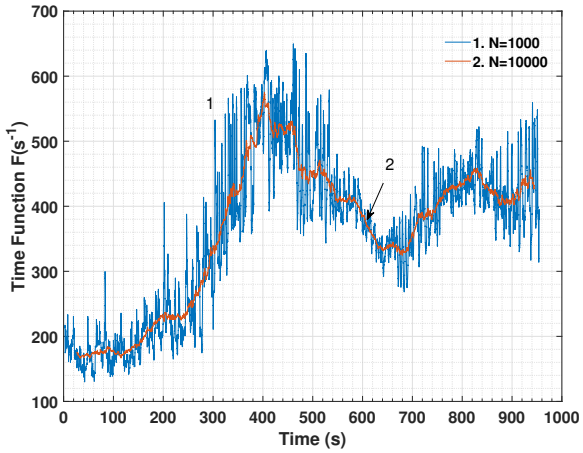

Figure 5: Effect of variation of N with time

5 CONCLUSIONS

The AE recorded during the compressive fracture of the SFRC is analyzed using time function analysis. The primary emphasis of this work lies in understanding time function $F(\tau)$ and its variation in accordance with the fracture mechanisms occurring in the uniaxial unconfined compression. The following major conclusions were drawn:

1. Microcracks dominate in the elastic compression and fiber-bridging regions.

2. The time function exhibits a power-law distribution. The exponent indicate the scaling by which the time function evolve with time to failure.

3. As the time of failure approaches, the rate of change of F reduces to almost equal to zero. This could be a pre-failure indication. Therfore, F can be a guiding tool for early fracture detection.

4. The optimum value of sliding time window is required to study the behavior of F. This is because increasing N enhances the resolution of the plots.

REFERENCES

[1] Balaguru, P.N. and Shah, S.P., 1992. *Fiber-reinforced cement composites.*

[2] Gopalaratnam, V.S., Shah, S.P., Batson, G., Criswell, M., Ramakishnan, V. and Wecharatana, M., 1991. Fracture toughness of fiber reinforced concrete. *Materials Journal,* **88(4)**,pp.339-353.

[3] Ohtsu, M., 2010. Measurement method for acoustic emission signals in concrete. *Materials and Structures,* **43**,pp.1177-1181.

[4] Ohtsu, M., 2010. Test method for classification of active cracks in concrete structures by AE. *Materials and Structures,* **43**,pp.1187-1189.

[5] Aggelis, D.G., Mpalaskas, A.C. and Matikas, T.E., 2013. Acoustic signature of different fracture modes in marble and cementitious materials under flexural load. *Mechanics Research Communications,* **47**, pp.39-43.

[6] Vallianatos, F., Benson, P., Meredith, P. and Sammonds, P., 2012. Experimental evidence of a non-extensive statistical physics behaviour of fracture in triaxially deformed Etna basalt using acoustic emissions. *Europhysics Letters,* **97(5)**, p.58002

[7] Salje, E.K., Planes, A. and Vives, E., 2017. Analysis of crackling noise using the maximum-likelihood method: Power-law mixing and exponential damping. *Physical Review E,* **96(4)**), p.042122

[8] Li, B., Xu, L., Shi, Y., Chi, Y., Liu, Q. and Li, C., 2018. Effects of fiber type, volume fraction and aspect ratio on the flexural and acoustic emission behaviors of steel fiber reinforced concrete. *Construction and Building Materials,* **181**, pp.474-486.

[9] Vidya Sagar, R., Ghosh, S., Kalloli, P.J. and Singh, M., 2021. Influence of fiber content on acoustic emission characteristics related to steel fiber–reinforced concrete subjected to unconfined uniaxial compression. *Journal of Materials in Civil Engineering,* **33(5)**, p.04021073.

[10] Behnia, A., 2015 *Characterization of fracture behavior of concrete structural elements using acoustic emission technique (Doctoral dissertation, University of Malaya).*

[11] Saha, I. and Sagar, R.V., 2021. Classification of the acoustic emissions generated during the tensile fracture process in steel fibre reinforced concrete using a waveform-based clustering method. *Construction and Building Materials,* **294**, p.123541.

[12] Sagar, R.V. and Prasad, B.R., 2012. A review of recent developments in parametric based acoustic emission techniques applied to concrete structures. *Nondestructive Testing and Evaluation,* **27(1)**, pp.47-68.

[13] Triantis, D. and Kourkoulis, S.K., 2018. An alternative approach for representing the data provided by the acoustic emission technique. *Rock Mechanics and Rock Engineering,* **51**, pp.2433-2438.

[14] Yang, L., Xie, H., Fang, S., Huang, C., Yang, A. and Chao, Y.J., 2021, June. Experimental study on mechanical properties and damage mechanism of basalt fiber reinforced concrete under uniaxial compression. *In Structures Elsevier,* **Vol. 31**, pp. 330-340.

[15] De Santis, A., Cianchini, G. and Di Giovambattista, R., 2015. Accelerating moment release revisited: Examples of application to Italian seismic sequences. *Tectonophysics,* **639**, pp.82-98.